RSC Advances

PAPER

View Article Online
View Journal | View Issue

Cite this: *RSC Adv.*, 2014, **4**, 48163

Synthesis, characterization, and computational study of potential itaconimide-based initiators for atom transfer radical polymerization†

Chetana Deoghare,[a] C. Baby,[b] Vishnu S. Nadkarni,[c] Raghu Nath Behera*[a] and Rashmi Chauhan*[a]

Atom transfer radical polymerization (ATRP) has been a promising technique to provide polymers with well-defined composition, architecture, and functionality. In most of the ATRP processes, alkyl halides are used as an initiator. We report the synthesis of three possible potential initiators, *N*-phenyl(3-bromo-3-methyl) succinimide, *N*-phenyl(3-bromo-4-methyl)succinimide, and *N*-phenyl(3-bromomethyl)succinimide for ATRP of *N*-phenylitaconimide (PI) and methyl methacrylate (MMA). These functionalized alkyl halides, having structural similarity with PI, were characterized by FTIR, HRMS, ^{1}H, ^{13}C NMR spectroscopy, and elemental analysis. The equilibrium constants for the ATRP activation/deactivation process (K_{ATRP}) of these alkyl halides as well as a commercial ATRP initiator (ethyl-α-bromoisobutyrate) were determined using UV-Vis-NIR and DOSY NMR spectroscopy. Alternatively, these compounds and similar alkyl halides (R-X) were investigated using density functional theory for their possible chain initiation activity for the ATRP process. The B3LYP functional and 6-31+G(d)/LanL2DZ basis set was used for the prediction of geometries and energetics associated with the homolytic R–X bond dissociation. The relative value of K_{ATRP} and its variation with system parameters (such as substituent, temperature, and solvent) was investigated. We found a good agreement between the experimentally determined and theoretically calculated K_{ATRP} values. Our experiments show that the newly synthesized initiator *N*-phenyl(3-bromo-3-methyl)succinimide performs better than the commercially available initiator ethyl-α-bromoisobutyrate for the atom transfer radical copolymerization of PI and MMA.

Received 20th August 2014
Accepted 2nd September 2014

DOI: 10.1039/c4ra08981b

www.rsc.org/advances

Introduction

Atom transfer radical polymerization (ATRP)[1] is a popular and robust controlled radical polymerization (CRP) technique for the preparation of polymers with controlled architecture and site-specific functionality. Like other CRP methods,[2–5] ATRP is controlled by the equilibrium between propagating radicals and dormant species (mostly in the form of initiating alkyl halides or macromolecular species).[6] Various types of initiators have been used in ATRP,[2,7,8] *e.g.*, halogenated alkanes, benzylic halides, α-haloesters, α-haloketones, α-halonitriles, sulfonyl halides, and iniferters. The basic mechanism of the ATRP process (Scheme 1) involves homolytic cleavage of the alkyl halide (R–X) bond (activation step) by a transition metal complex in its lower oxidation state (the activator, M_t^nY/L), reversibly generating (with rate constant of activation, k_{act}) the propagating radical ($R^\bullet$) and the transition metal halide complex in its higher oxidation state (the deactivator, $X–M_t^{n+1}Y/L$). In the deactivation step (with rate constant of deactivation, k_{deact}), the halide atom (X) is transferred back from the activator to the propagating radical, also through homolytic bond dissociation.[9]

A successful ATRP process requires uniform growth of all the chains and small contribution of the terminated chain. This can be achieved through fast initiation and rapid reversible deactivation and also by preserving the chain end functionality.[10] For

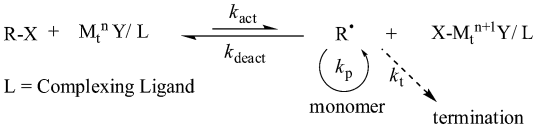

Scheme 1 Mechanism of transition metal-catalyzed ATRP.

[a]*Department of Chemistry, Birla Institute of Technology and Science, Pilani – K. K. Birla Goa Campus, Zuarinagar – 403726, Goa, India. E-mail: rbehera@goa.bits-pilani.ac.in; rchauhan@goa.bits-pilani.ac.in; Fax: +91 832 2557033; Tel: +91 832 2580331/153*

[b]*Sophisticated Analytical Instrument Facility, Indian Institute of Technology Madras, Chennai, Tamilnadu – 600036, India*

[c]*Department of Chemistry, Goa University, Taleigao Plateau, Goa – 403206, India*

† Electronic supplementary information (ESI) available: Supplementary data associated with this manuscript: FTIR, ^{1}H, ^{13}C NMR, and HRMS spectra of synthesized alkyl bromides; graphs related to the experimental determination of the equilibrium constant of ATRP; and ^{1}H NMR spectra of reaction mixture of copolymers of PI and MMA. B3LYP/6-31+G(d)/LanL2DZ optimized the gas phase geometries of all the studied compounds. See DOI: 10.1039/c4ra08981b

an ATRP initiator to be efficient, the rate of initiation should be faster than the rate of propagation, and there should be minimum side reactions. However, a very reactive initiator may provide too many radicals that will terminate in the early stage and slow down the overall process. Thus, the initiator reactivity should be comparable to the monomer reactivity. One way of achieving this is to employ an initiator that structurally mimics the dormant species.[2,6,11] To obtain a well-defined polymer with narrow molecular distribution, the halide group must rapidly and selectively migrate between the growing chain and the transition metal complex (the catalyst). Thus, the initiator should be carefully selected in accordance with the structure and reactivity of the monomers and metal complexes.[12] A normal ATRP process has one notable limitation in that the catalysts used are sensitive to air and other oxidants.[13] In order to overcome this drawback, Matyjaszewski's group[14] has developed an improved ATRP technique, namely, an activator generated by electron transfer atom transfer radical polymerization (AGET-ATRP). In a typical AGET-ATRP system, a transition metal complex in its higher oxidation state such as Cu^{II} complex is used as a catalyst instead of Cu^{I} complex for a normal ATRP system. The Cu^{I} complex is generated *in situ* from Cu^{II} complex using a reducing agent such as tin(II)-ethylhexanoate.[14a]

Several experimental[15] as well as theoretical[15b,16] studies have reported the kinetic and thermodynamic parameters of ATRP for various systems. The rate of an ATRP process depends on the concentration of monomer [M] and propagating radical [P$^{\bullet}$]. The radical concentration depends on the position of the equilibrium and equilibrium constant of ATRP ($K_{ATRP} = k_{act}/k_{deact}$). Experimentally, K_{ATRP} can be determined from the polymerization kinetics. For example, in a Cu^{I}Y/L (Y = Cl/Br)-catalyzed polymerization reaction when excess deactivating species (X-Cu^{II}L) is used and the concentration of other species such as activator, initiator, and monomer do not change significantly, the rate of propagation (R_p) is given as[17]

$$R_p = k_p[M][P^{\bullet}] = k_p K_{ATRP}[M][I]_0 \times [Cu^{I}Y/L]/[X\text{-}Cu^{II}L] \quad (1)$$

where k_p = rate constant of propagation, $[I]_0$ = initial concentration of initiator R–X, and [Cu^{I}] = concentration of activator. Using eqn (1), K_{ATRP} can be determined provided that k_p is known.

Alternatively, K_{ATRP} can also be determined from the rate of formation of a dormant species/persistent radical using the Fischer–Fukuda equation for the persistent radical effect (eqn (2) and (3)):[15b,18]

$$Y = (6k_t(K_{ATRP})^2 I_0^2 C_0^2)^{1/3} t^{1/3}. \quad (2)$$

$$R = \left(\frac{K_{ATRP} I_0 C_0}{6k_t}\right)^{1/3} t^{-1/3} \quad (3)$$

The Fischer–Fukuda equation can be modified[15b,19] to take into account the changes in catalyst and initiator concentration (eqn (4)–(6)):

$$F(Y) = 2k_t(K_{ATRP})^2 t + c' \quad (4)$$

where,

$$F(Y) = \left(\frac{I_0 C_0}{C_0 - I_0}\right)^2 \left(\frac{1}{C_0^2(C_0 - Y)} + \frac{2}{I_0 C_0 (C_0 - I_0)} \ln\left(\frac{I_0 - Y}{C_0 - Y}\right) + \frac{1}{I_0^2 (C_0 - Y)}\right) \text{ for } C_0 \neq I_0 \quad (5)$$

and,

$$F(Y) = \frac{C_0^2}{3(C_0 - Y)^3} - \frac{C_0}{(C_0 - Y)^2} + \frac{1}{C_0 - Y} \text{ for } C_0 = I_0 \quad (6)$$

In the above eqn (2)–(6), Y = concentration of deactivating species (X-Cu^{II}L), I_0 = initial concentration of initiator (R–X), C_0 = initial concentration of catalyst (Cu^{I}Y/L), R is the concentration of radical (R$^{\bullet}$), k_t is the termination rate constant, and t is time. The K_{ATRP} can be calculated (eqn (4)) from the slope of the plot $F(Y)$ *vs.* t $\left(K_{ATRP} = \sqrt{\frac{\text{slope}}{2k_t}}\right)$, provided that k_t is known.

Theoretically, the relative values of K_{ATRP} can be estimated from the homolytic bond dissociation energy (BDE) of the initiating R–X under certain conditions.[20] The atom transfer equilibrium of the ATRP process.

$$(ii)\, M_t^{\,n}Y/L + X^{\cdot} \overset{K_X}{\rightleftharpoons} X - M_t^{\,n+1}Y/L \quad (7)$$

can be viewed as the sum of the following two equilibrium processes,[7,9] *viz.* (i) the homolytic bond dissociation of alkyl halide (eqn (8)) and (ii) X–M_t^{n+1}Y/L bond formation (*halidophilicity*, eqn (9)), so that $K_{ATRP} = K_{RX} \times K_X$.

$$(i)\ R - X \overset{K_{RX}}{\rightleftharpoons} R^{\cdot} + X^{\cdot} \quad (8)$$

$$(ii)\ M_t^{\,n}Y/L + X^{\cdot} \overset{K_X}{\rightleftharpoons} X - M_t^{\,n+1}Y/L \quad (9)$$

The value of the equilibrium constant K_X depends on the type of catalyst/ligand (M_t^{n}Y/L) and halogen, X. For similar conditions and using the same catalytic system (similar K_X), the overall equilibrium constant K_{ATRP} will depend on the energetics of alkyl halide R–X, and a knowledge of the equilibrium constant K_{RX} alone will enable prediction of the relative value of K_{ATRP}.[9,20a,20b]

Several studies have been performed on ATRP of methyl methacrylate (MMA) using ethyl-α-bromoisobutyrate (**4**-Br) as the initiator.[21] We are interested in the copolymerization of *N*-phenylitaconimide (PI) and MMA. Recently, we used the ATRP method to copolymerize PI with MMA (in anisole at 80 °C using CuBr/bipyridine catalyst) using the commercially available initiator **4**-Br, which resembles the monomer MMA.[22] The molecular weight of the obtained copolymer was found to be less (3412 g mol^{-1}) than that obtained by a conventional polymerization method (23 300 g mol^{-1}),[23] which may have

occurred due to the chosen initiator. Previous studies[23,24] on such copolymer systems have shown higher reactivity ratios for itaconimides monomers as compared to MMA. This necessitates the need to explore *de novo* initiators for ATRP of PI and MMA. It will be of interest to copolymerize the same system with different initiators obtained from renewable resources that have structural similarities with the other monomer (*i.e.*, the itaconimide).

In this study, we report the synthesis of three alkyl halides [*N*-phenyl(3-bromo-3-methyl)succinimide, *N*-phenyl(3-bromo-4-methyl)succinimide, and *N*-phenyl(3-bromomethyl)succinimide] that are structurally similar to PI. These alkyl halides were prepared from itaconic acid.[25] The K_{ATRP} values of the synthesized alkyl halides and **4**-Br were determined using UV-Vis-NIR spectroscopy. These alkyl halides, as well as some similar halides and some well-known ATRP initiators, were also investigated using density functional theory (DFT) before attempting to use them as initiators for the ATRP copolymerization. The predicted initiator, *N*-phenyl(3-bromo-3-methyl)succinimide, was successfully tested for the copolymerization of PI and MMA *via* the AGET-ATRP process.

Experimental section

Chemicals and materials

Itaconic acid (99.0%) and phosphorus pentoxide (95.0%) were used as supplied; chloroform (99.5%), acetic anhydride (98%), aniline (99.5%), and acetone (99.0%) were purified by distillation. Anhydrous sodium acetate (99.5%) was dried over flame. Silica gel for column chromatography was used as supplied. Dichloromethane (DCM, 99.0%) and toluene (99.0%) were dried using fused calcium chloride and purified by distillation. 2,2′-Bipyridine (Bpy) (99.5%) and acetonitrile dry (99.5%) were used as supplied. All of the above chemicals were obtained from S. D. Fine Chem Limited, Mumbai, India. Itaconic anhydride (**I**) was synthesized from itaconic acid using the known methods previously reported.[26] HBr gas was prepared by the bromination of 1,2,3,4-tetrahydro-naphthalene (99.0%, Sigma-Aldrich, Bangalore, India) with bromine (95.0%, S. D. Fine Chem Limited, Mumbai, India) using a previously published procedure.[27] Ethyl-α-bromoisobutyrate (98.0%), $CuBr_2$ (99.9%), and tin(II) ethylhexanoate [$Sn(EH)_2$] (95.0%) were obtained from Sigma-Aldrich Chemicals Private Limited, Bangalore, India and used as supplied. CuBr (99.9%, Sigma-Aldrich Chemicals Private Limited, Bangalore, India) was purified by stirring overnight in glacial acetic acid and washing with absolute ethanol and diethyl ether, followed by drying under vacuum. Methyl methacrylate (99.0%, S. D. Fine Chem Limited, Mumbai, India) was purified by washing with 5% NaOH solution to remove the inhibitor, followed by repeated washing with distilled water until the pH was neutral. It was then kept on anhydrous magnesium sulfate to remove any traces of water followed by vacuum distillation with calcium hydride. Anisole (99.0%, SRL Private limited, Mumbai, India) was purified by washing with 5% NaOH solution and then with distilled water. It was then kept on anhydrous potassium carbonate to remove any traces of water, followed by vacuum distillation over sodium benzophenone.

The FTIR spectra were recorded on a Shimadzu DR-8031 FTIR spectrophotometer in the region from 4000 to 400 cm^{-1} using a KBr pellet. The ^1H NMR and ^{13}C NMR spectra were obtained by dissolving the samples in deuterated chloroform ($CDCl_3$) using a Brucker AV III 500 MHz FT-NMR and a Brucker DRX500 spectrometer, respectively. Chemical shifts (δ) are given relative to tetramethylsilane (TMS). Diffusion ordered spectroscopy (DOSY) NMR measurements were performed on a Bruker Avance (AV III) 500 MHz NMR spectrometer, equipped with a 5 mm broadband observe (BBO) *z*-axis gradient probe which delivers a maximum gradient strength of 50 G cm^{-1}. Experiments were carried out with active temperature regulation at 25 °C. Self-diffusion coefficients were measured using the stimulated echo, bipolar gradient (stebpgp1s) pulse sequence. Generally, the diffusion coefficient (D) is experimentally determined by monitoring the signal intensity decay in a 1D pulsed-field gradient spin-echo experiment (PFGSE) spectrum as a function of the applied gradient strength.[28] In the two-dimensional DOSY experiment,[29,30] the decay of magnetization as a function of increasing gradient intensity (*i.e.*, the gradient ramp) was observed. The gradient ramp in our experiment was adjusted between 2 and 95% strength of the gradient amplifier using 16 equidistant steps. Each experiment was acquired with a spectral width of 4500 Hz and 16k complex points. A diffusion time (Δ) of 100 ms was used, and the duration of the gradient pulse (δ) was 1 ms. After Fourier transform and baseline correction, the spectra were processed with DOSY processing tools from the Bruker Topspin 2.1 software package. The data were analyzed using variable gradient fitting routines, and in all cases, the proton resonances were fit with a single exponential decay function using peak intensities. HRMS was recorded using the 1290 Infinity UHPLC System, 1260 Infinity Nano HPLC with Chipcube, and 6550 iFunnel Q-TOF. Elemental analysis of the compounds was done using a Vario Micro Cube elemental analyzer. The spectroscopic measurements were obtained with a Jasco V-570 UV-Vis-NIR spectrometer. Molecular-mass characteristics of the copolymers were determined by gel permeation chromatography (GPC) in THF as an eluent at a flow rate of 0.75 mL min^{-1} and column temperature of 25 °C with an Agilent 1260 HPLC-GPC system equipped with column: PL gel 5 micron Mixed D: 300 mm × 7.5 mm with a differential refractometer. Polystyrene standards with a molecular weight of 10^3 to 10^5 g mol^{-1} were used for calibration.

Computational details

Gaussian09 [31] was used as the source program for all theoretical calculations. All the geometries were fully optimized using the hybrid B3LYP exchange correlation functional[32] with the 6-31+G(d) basis set, except for iodine, where we used the LanL2DZ basis set. Frequency calculations were performed for all the compounds to confirm (no imaginary frequencies) the stationary points as minima on the potential energy surface. The scaling factor used for the frequency calculation was 0.9613.[33] We have used the Gauge-Independent Atomic Orbital

(GIAO) method inbuilt in the Gaussian09 software for computing NMR properties. All of the ^{1}H NMR calculations were carried out using the HF/6-311+G(2d,p) method from B3LYP/6-31+G(d) optimized geometry. All the systems containing unpaired electrons were optimized with spin unrestricted formalism. The spin contamination was found to be negligible (the mean value of the S^2 operator was close to the theoretical value of 0.75 for all radicals). A spin–orbit correction term was applied for X = Cl, Br, and I due to their atomic nature.[34] The DFT calculation includes only the average energy of the ground state ^{2}P term; the extra stability of the real ground-state $^2P_{3/2}$ term is taken from the literature values (0.8, 3.5, and 7.3 kcal mol^{-1} for Cl, Br, and I respectively).[35] Solvent effects were studied using Tomasi's polarizable continuum model (PCM).[35]

A. Synthesis of compounds II–IV (Scheme 2)

1. Synthesis of N-phenylitaconamic acid (II). In a one-litre kettle equipped with a mechanical stirrer, **I** (30 g, 0.27 mol) was dissolved in 100 mL of acetone. To this solution, aniline (25 mL, 0.27 mol), dissolved in 100 mL of acetone, was slowly added with vigorous stirring. After the *N*-phenylitaconamic acid started precipitating out, the stirring was continued for another 12 h. The obtained precipitate was filtered, dissolved in a saturated solution of sodium bicarbonate, and reprecipitated with 5 M HCl. The precipitate was filtered, washed with distilled water, and dried in an oven at 80 °C, giving **II** (19.0 g, yield 63%, mp 145–150 °C).

2. Synthesis of N-phenylitaconimide (III) and N-phenylcitraconimide (IV). To the solution of **II** (25 g, 0.14 mol) in 100 mL of acetone, acetic anhydride (25 mL, 0.25 mol) and anhydrous sodium acetate (10 g, 0.12 mol) were added. The reaction mixture was refluxed until a clear solution was obtained, and refluxing with stirring was continued for another 5 h. The reaction mixture was then cooled to room temperature and poured in an excess of ice cold water. The precipitate obtained was filtered and washed with a saturated solution of sodium bicarbonate followed by distilled water. The crude product was purified by column chromatography using 10% ethyl acetate in hexane as the eluent, giving **III** and **IV** Scheme 2.

N-Phenylitaconimide (III), (12.5 g, yield 50%, mp 115 °C). IR (KBr, cm^{-1}): 3098 (aromatic C–H stretch), 3050 (alkenyl C–H stretch), 2994, 2955 (C–H stretch), 1789 and 1714 (>C═O of imide), 1663 (>C═C< stretch of double bond in ring), 1593, 1501, 1453 (aromatic >C═C< stretch), 761 (oop C–H bending).

^{1}H NMR ($CDCl_3$) δ: 7.4 (m, 2H, C_6H_5), 7.3 (m, 2H, C_6H_5), 7.2 (m, 1H, C_6H_5), 6.4 (m, 1H, H1 of vinylic CH_2), 5.6 (m, 1H, H2 of vinylic CH_2), 3.4 (m, 2H, CH_2 of ring).

N-Phenylcitraconimide (IV), (6.2 g, yield 25%, mp 100 °C). IR (KBr, cm^{-1}): 3082 (aromatic C–H stretch), 3069 (alkenyl C–H stretch), 2923 (C–H stretch), 1701 and 1717 (>C═O of imide), 1641 (>C═C< stretch of double bond in ring), 1593, 1505, 1409 (aromatic >C═C< stretch), 876 (oop C–H bending).

^{1}H NMR ($CDCl_3$) δ: 7.4 (m, 2H, C_6H_5), 7.3 (m, 2H, C_6H_5), 7.2 (m, 1H, C_6H_5), 6.4 (q, 1H, ^3J = 1.6 Hz, CH), 2.1 (d, 3H, ^3J = 1.6 Hz, CH_3).

The FTIR and ^{1}H NMR spectra of compounds **III** and **IV** are given in ESI Fig. S1 to S4.† The detailed characterization of compounds **III** and **IV** has previously been reported.[23,36]

B. Synthesis of bromo substituted succinimides (Scheme 3)

*3. Preparation of N-phenyl(3-bromomethyl)succinimide (**1a**-Br).* To the solution of **III** (2 g, 0.01 mol) in 50 mL of toluene, HBr gas was purged for 24 h at 80 °C in the presence of benzoyl peroxide, with continuous stirring that was extended for an additional 12 h. The crude product obtained by concentrating the reaction mixture with a rotary evaporator was purified by column chromatography using petroleum ether and diethyl ether as the solvent system, followed by crystallization with DCM and hexane. The compound was dissolved in a minimal amount of DCM, and hexane was added dropwise until the solution was turbid. The mixture was then kept on ice to obtain crystals of **1a**-Br (1.0 g, yield 50%, mp 177 °C).

IR (KBr, cm^{-1}): 3069 (aromatic C–H stretch), 1784, and 1703 (>C═O of imide), 1590, 1491, and 1447 (aromatic >C═C< stretch), 758 (oop C–H bending), 595 (C–Br stretch).

^{1}H NMR ($CDCl_3$) δ: 7.3 (m, 1H, C_6H_5), 7.4 (m, 2H, C_6H_5), 7.5 (m, 2H, C_6H_5), 4.0 (dd, 1H, ^1J = 8.4 Hz, ^2J = 4.5 Hz, CH_2), 3.7 (dd, 1H, ^1J = 8.4 Hz, ^2J = 3.5 Hz, CH_2), 3.5 (m, 1H, CH), 2.9 (dd, 1H, ^1J = 14.8 Hz, ^2J = 5.0 Hz, CH_2), 3.1 (dd, 1H, ^1J = 14.8 Hz, ^2J = 9.5 Hz, CH_2).

^{13}C NMR (125 MHz, $CDCl_3$) δ: 175.81 and 174.52 (>C═O), 129.33, 128.97, 128.52, and 131.74 (C_6H_5), 41.20 (CH_2Br), 33.38 (CH), 32.32 (CH_2).

Elemental analysis (CHNOBr): found – %C, 49.02; %H, 3.71; %N, 5.13; %O, 11.88; %Br, 30.26; calculated for $C_{11}H_{10}NO_2Br$: %C, 49.28; %H, 3.76; %N, 5.22; %O, 11.94; %Br, 29.80.

HRMS (EI): (m/z) 267.7751 ([M]$^+$; 95%), 269.4687 ([M + 2]$^+$; 90%); calculated mass for $C_{11}H_{10}NO_2Br$; 268.1066, observed mass for $C_{11}H_{10}NO_2Br$; 268.6219.

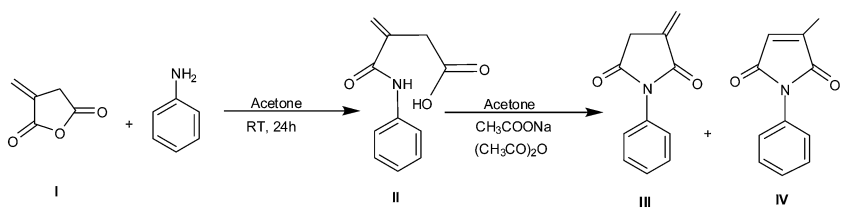

Scheme 2 Synthesis of *N*-phenylitaconimide (III) and *N*-phenylcitraconimide (IV).

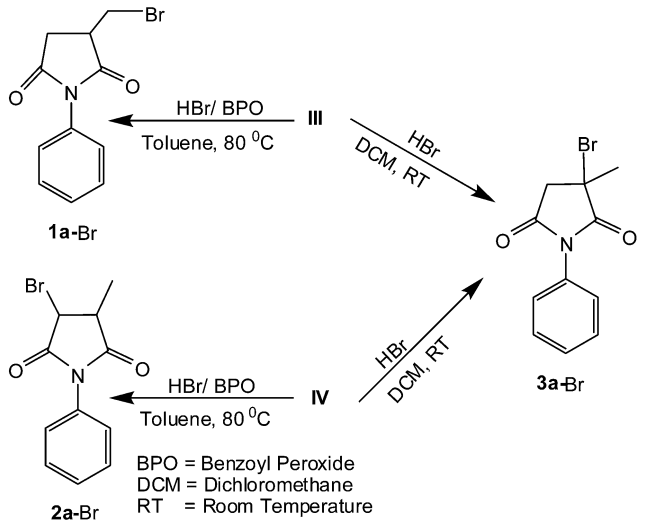

Scheme 3 Synthesis of bromo-substituted succinimides.

*4. Preparation of N-phenyl(3-bromo-4-methyl)succinimide (**2a**-Br).* To the solution of **IV** (2 g, 0.01 mol) in 50 mL of toluene, HBr gas was purged for 24 h at 80 °C in the presence of benzoyl peroxide, with continuous stirring that was extended for an additional 12 h. The crude product obtained by concentrating the reaction mixture with a rotary evaporator was purified by column chromatography using petroleum ether and diethyl ether as the solvent system, followed by crystallization with DCM and hexane. The compound was dissolved in a minimal amount of DCM, and hexane was added dropwise until the solution was turbid. The mixture was then kept on ice to obtain crystals of **2a**-Br (1.3 g, yield 65%, mp 116 °C).

IR (KBr, cm^{-1}): 3077 (aromatic C–H stretch), 1791 and 1716 (>C═O of imide), 1591, 1501 and 1444 (aromatic >C═C< stretch), 763 (oop C–H bending), 520 (C–Br stretch).

^{1}H NMR ($CDCl_3$) δ: 7.3 (m, 1H, C_6H_5), 7.4 (m, 2H, C_6H_5), 7.5 (m, 2H, C_6H_5), 4.9 (d, 1H, ^2J = 7.6 Hz, CH), 3.3 (m, 1H, CH), 1.5 (d, 3H, ^2J = 7.2 Hz, CH_3).

^{13}C NMR (125 MHz, $CDCl_3$) δ: 174.74 and 171.65, 131.45, 129.37, 129.07, and 126.28 (C_6H_5), 48.29 (C–Br), 40.68 (CH), 14.47 (CH_3).

Elemental analysis (CHNOBr): found – %C, 49.27; %H, 3.76; %N, 5.04; %O, 11.92; %Br, 30.01; calculated for $C_{11}H_{10}NO_2Br$: %C, 49.28; %H, 3.76; %N, 5.22; %O, 11.94; %Br, 29.80.

HRMS (EI): (m/z) 267.9651 ($[M]^+$; 60%), 269.4657 ($[M + 2]^+$; 60%); calculated mass for $C_{11}H_{10}NO_2Br$; 268.1066, observed mass for $C_{11}H_{10}NO_2Br$; 268.7154.

*5. Preparation of N-phenyl(3-bromo-3-methyl)succinimide (**3a**-Br).* To the solution of **III** or **IV** (2 g, 0.01 mol) in 50 mL of DCM, HBr gas was purged for 24 h at room temperature in the absence of benzoyl peroxide, with continuous stirring that was extended for 12 h. The crude product obtained by concentrating the reaction mixture with a rotary evaporator was purified by column chromatography using petroleum ether and diethyl ether as the solvent system, followed by crystallization with DCM and hexane. The compound was dissolved in a minimum amount of DCM, and hexane was added dropwise until the solution was turbid. The mixture was then kept on ice to obtain crystals of **3a**-Br (1.3 g, yield 65%, mp 109 °C).

IR (KBr, cm^{-1}): 3048 (aromatic C–H stretch), 1751 and 1714 (>C═O of imide), 1591, 1501 and 1452 (aromatic >C═C< stretch), 760 (oop C–H bending), 512 (C–Br stretch).

^{1}H NMR ($CDCl_3$) δ: 7.3 (m, 1H, C_6H_5), 7.4 (m, 2H, C_6H_5), 7.5 (m, 2H, C_6H_5), 3.5 (d, 1H, ^1J = 18.8 Hz, CH_2), 3.2 (d, 1H, ^1J = 18.8 Hz, CH_2), 2.1 (s, 3H, CH_3).

^{13}C NMR (125 MHz, $CDCl_3$) δ: 174.74 and 171.65, 131.47, 129.34, 129.04, and 126.26 (C_6H_5), 51.29 (C–Br), 47.68 (CH_2), 27.47 (CH_3).

Elemental analysis (CHNOBr): found – %C, 50; %H, 3.82; % N, 5.36; %O, 12.05; %Br, 28.77; calculated for $C_{11}H_{10}NO_2Br$: % C, 49.28; %H, 3.76; %N, 5.22; %O, 11.94; %Br, 29.80.

HRMS (EI): (m/z) 267.8351 ($[M]^+$; 25%), 269.4401 ($[M + 2]^+$; 25%); calculated mass for $C_{11}H_{10}NO_2Br$; 268.1066, observed mass for $C_{11}H_{10}NO_2Br$; 268.5376.

The FTIR, ^{1}H, ^{13}C NMR, and HRMS data of synthesized compounds **1a**-Br, **2a**-Br, and **3a**-Br are given in ESI Fig. S5 to S16.†

C. Synthesis of copolymers of PI and MMA using *N*-phenyl(3-bromo-3-methyl)succinimide as the initiator. The reaction for the synthesis of copolymers of PI and MMA using AGET-ATRP is shown in Scheme 4. A solution of PI (1.87 g, 0.01 mol) and MMA (4.0 mL, 0.04 mol) in 10 mL of dry anisole was poured into a three-neck 100 mL round-bottom flask equipped with a reflux condenser and a magnetic bead. To this reaction mixture, $CuBr_2$ (56 mg, 0.25 mmol), $Sn(EH)_2$ (41 μL, 0.125 mmol), and 2,2′-bipyridine (117.14 mg, 0.75 mmol) were added. The reaction mixture was frozen under nitrogen, thawed, and degassed under vacuum; this cycle was repeated twice. **3a**-Br (67 mg, 0.25 mmol) was dissolved in 4 mL of dry anisole in a separate two-neck 100 mL round-bottom flask and was degassed with a freeze–pump–thaw cycle twice, and was then charged to the three-neck reaction flask through a nitrogen-purged syringe. The mixture was again subjected to a freeze–thaw–vacuum cycle three times. The reaction flask was now immersed in a hot oil bath maintained at 80 °C. The polymerization was terminated by adding the reaction mixture in excess of methanol. The copolymer that precipitated out was filtered and washed with hot methanol to remove any unreacted monomers. The obtained copolymer was dissolved in 100 mL acetone and passed through an alumina bed to remove the catalyst. It was concentrated using a rotary evaporator and reprecipitated with methanol. The obtained copolymer was

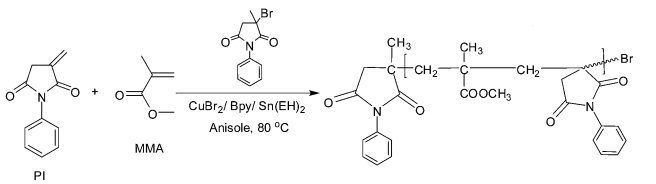

Scheme 4 Reaction scheme for the synthesis of copolymer of PI and MMA *via* AGET-ATRP using **3a**-Br as the initiator.

then dried under vacuum. The final yield of the copolymer was obtained using a gravimetric method. The reactions under similar conditions were carried out in ten different reaction flasks and quenched at different time intervals, *i.e.*, 5 h, 10 h, 15 h, 20 h, 25 h, 30 h, 35 h, 45 h, and 50 h.

D. Determination of the ATRP equilibrium constant (K_{ATRP}). The K_{ATRP} of the studied alkyl bromides were determined using eqn (4) and (5). In these equations, the parameters I_0 and C_0 are known, and Y = [BrCu^{II}Bpy] and k_t are determined as follows.

6. Determination of [BrCu^{II}Bpy]. To a dry, three-neck round-bottom flask, dry acetonitrile (30 mL) was added, and nitrogen was bubbled for five min. Cu^{I}Br (15.06 mg, 3.7 mM) and the ligand Bpy (32.80 mg, 7.0 mM) were then added to the flask, and the contents were stirred for 30 minutes to ensure complete dissolution of Cu^{I}Br and formation of complex. The absorbance of the obtained solution (at λ = 745 nm for BrCu^{II}Bpy complex) was set to zero. To this solution, **4**-Br (70 mM, 308 μL) was added, and the resulting mixture was stirred at room temperature (25 °C). The absorbance of this solution was measured after every 15 min. A linear increase in the absorbance was observed, which indicated an increase in the concentration of the BrCu^{II}Bpy complex. The same experiment was repeated using 50 mM of **4**-Br.

Similarly, the same experiments were performed using all other synthesized alkyl bromides, *viz.* **1a**-Br, **2a**-Br, and **3a**-Br, at two different concentrations (*i.e.*, 70 mM and 50 mM). The plots of absorbance *vs.* time at 745 nm are given in ESI Fig. S17 to S20.† The concentration of the BrCu^{II}Bpy complex was determined using values of the extinction coefficient for the BrCu^{II}Bpy complex, which were determined separately.

To determine the extinction coefficient, different solutions of BrCu^{II}Bpy complex in acetonitrile were prepared, with known concentrations ranging from 0.2 mM to 4.6 mM. The absorbance for each solution was measured using a quartz cuvette at λ_{max} = 745 nm. The extinction coefficient calculated from the slope of the curve in the plot of concentration *vs.* absorbance (ESI Fig. S21†) was found to be 327 M^{-1} cm^{-1}.

7. Determination of termination rate constant (k_t). In the literature,[37] a constant value (2.5×10^9 M^{-1} s^{-1}) of k_t has been assumed for small radicals in the calculation of K_{ATRP}. However, a more accurate value can be theoretically calculated using the following formula:[38]

$$2k_t^D = 3.78 \times 10^{21} \times D \times d \quad (10)$$

where D is the diffusion coefficient of the radical in a given medium and d is the reaction distance. The latter parameter can be approximated using the approach of Gorrell and Dubois,[19,39] according to the equation

$$d = \left(\frac{V_m}{N_A}\right)^{1/3} \quad (11)$$

where V_m is the molar formula of a stable model compound structurally resembling the radical, and N_A is Avogadro's number. We used *N*-phenylsuccinimide (SI) as our model compound for the above synthesized alkyl halides. Taking its molecular weight (M = 175.18 g mol^{-1}) and density (ρ = 1.28 g cm^{-3}), the molar volume can be calculated as $V_m = M/d$ = 136.97 cm^3 mol^{-1}, and using eqn (11), a value of $d = 6.11 \times 10^{-8}$ cm is obtained. With this estimation of the reaction distance (d), eqn (10) can be rewritten (for the phenylsuccinimide radical) as:

$$2k_t^D = 2.31 \times 10^{14} \times D. \quad (12)$$

The diffusion coefficient D can be obtained from the classic Einstein–Stokes equation or some of its variations[40] or it can be directly calculated using pulsed field gradient NMR spectroscopic techniques.[41] The latter and more accurate approach was employed in the present study. DOSY allows the measurement of translational diffusion of molecules in solution. The measurement of diffusion is carried out by observing the attenuation of the NMR signals during a pulsed field gradient experiment. The degree of attenuation is a function of the magnetic gradient pulse amplitude and occurs at a rate proportional to the diffusion coefficient of the molecule. In practice, a series of NMR diffusion spectra are acquired as a function of the gradient strength. It can be observed that the intensities of the resonances follow an exponential decay. The slope of this decay is proportional to the diffusion coefficient according to the equation.

$$I = I_0 \exp(-D\gamma^2 g^2 \delta^2 \Delta - \delta/3 - \pi/2 \quad (13)$$

where I and I_0 are the signal intensities in the presence and absence of gradient, respectively, γ is the gyromagnetic ratio, g is the strength of the diffusion gradients, D is the diffusion coefficient of the observed spins, δ is the duration of the diffusion gradient, and Δ is the diffusion time. All signals corresponding to the same molecular species will decay at the same rate. The processing software evaluates this decay behavior and extracts the diffusion coefficient out of the signal decay curve. In two-dimensional DOSY NMR, spectra are presented with the chemical shift along the *x*-axis and the diffusion constant along the *y*-axis. The DOSY NMR spectrum of SI and its diffusion variable gradient are given in ESI Fig. S22 to S24.† From these data, the diffusion coefficient of SI in deuterated acetonitrile was found to be 1.65×10^{-5} cm^2 s^{-1}. Correspondingly, the value of the termination rate constant $2k_t$ for SI in deuterated acetonitrile at 25 °C was obtained as 3.81×10^9 M^{-1} s^{-1}, which is similar to the value used in the literature. This value of $2k_t$ was used for the determination of the K_{ATRP} values using acetonitrile as the solvent for the above synthesized alkyl bromides.

8. Determination of K_{ATRP} using UV-Vis-NIR spectroscopy. The K_{ATRP} values of the above synthesized alkyl bromides, *i.e.*, **1a**-Br, **2a**-Br, **3a**-Br and commercially available **4**-Br, were determined using the modified Fischer–Fukuda equation for the persistent radical effect (eqn (4)). The values of F(BrCu^{II}Bpy) were obtained by substituting the values for the concentration of Y, C_0 and I_0 into eqn (4). The plots of F(BrCu^{II}Bpy) *vs.* time (t) are linear in nature for all the above mentioned alkyl bromides, and these are given in Fig. 1 for the 70 mM concentration. Similar plots for the 50 mM concentration are given in ESI Fig. S25.† The K_{ATRP}

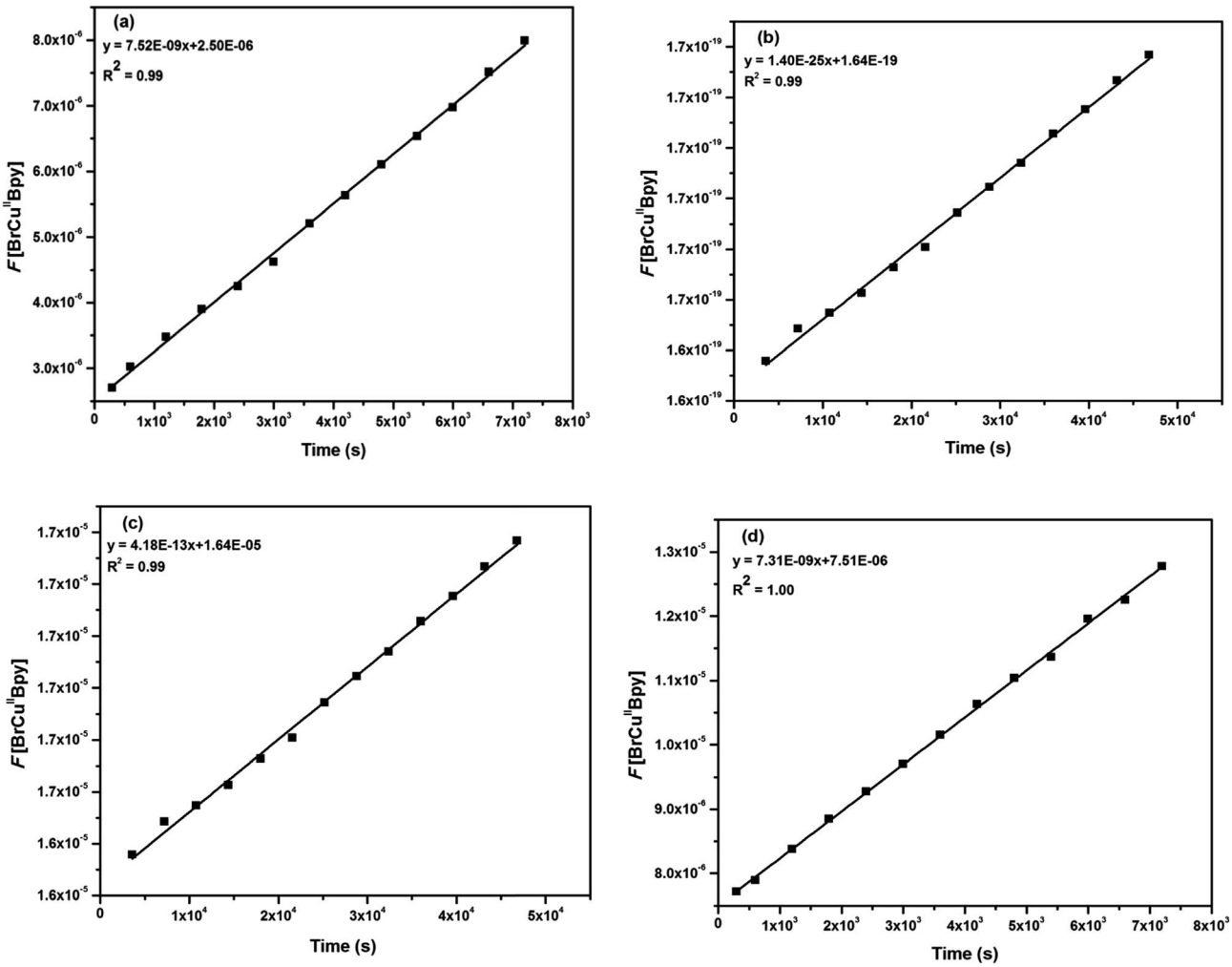

Fig. 1 Plots of $F(Y) = F[BrCu^{II}Bpy]$ *vs.* time (s) for the alkyl bromides at 70 mM, (a) **4**-Br, (b) **1a**-Br, (c) **2a**-Br, and (d) **3a**-Br.

Table 1 The K_{ATRP} values for R–X homolytic bond cleavage of the studied alkyl bromides in acetonitrile at 25 °C determined using UV-Vis-NIR spectroscopy. Experimental conditions: [R–X] : [CuBr] : [Bpy] = 70 and 50 mM : 3.5 mM : 7.0 mM. The K_{ATRP} values, calculated using DFT method, are given in the last column

R–X	K_{ATRP} at 70 mM	K_{ATRP} at 50 mM	Average K_{ATRP}	K_{ATRP} calculated
4-Br	1.40×10^{-09}	1.18×10^{-09}	1.29×10^{-09}	3.93×10^{-09}
1a-Br	0.89×10^{-18}	1.39×10^{-18}	1.14×10^{-18}	2.77×10^{-18}
2a-Br	1.07×10^{-11}	1.29×10^{-11}	1.18×10^{-11}	1.37×10^{-11}
3a-Br	1.39×10^{-09}	1.40×10^{-09}	1.40×10^{-09}	1.42×10^{-09}

values of synthesized alkyl bromides, *i.e.*, **1a**-Br, **2a**-Br, **3a**-Br, and commercially available **4**-Br, were determined from the slope (plot of $F(BrCu^{II}Bpy)$ *vs.* t) and the above calculated value of $2k_t$. The results are summarized in Table 1.

Results and discussion

In this work, we report the synthesis of compounds **1a**-Br and **2a**-Br by the hydrobromination of **III** and **IV**, respectively, with HBr gas in the presence of benzoyl peroxide at 80 °C using toluene as the solvent, while compound **3a**-Br was synthesized by the hydrobromination of **III** or **IV** with HBr gas in the absence of benzoyl peroxide at room temperature using DCM as the solvent. The hydrobromination reaction follows Markovnikov's addition (electrophilic addition reaction) of HBr across the double bond in the absence of peroxide and anti-Markovnikov's addition (free radical addition reaction) of HBr in the presence of peroxide.[42]

We also studied the bond dissociation enthalpies (BDEs) and other energetics for the four series of alkyl halides **1**, **2**, **3**, and **4** (Fig. 2). The chosen test set of alkyl halides includes (a) species that mimic the dormant chain ends in the polymerization of PI

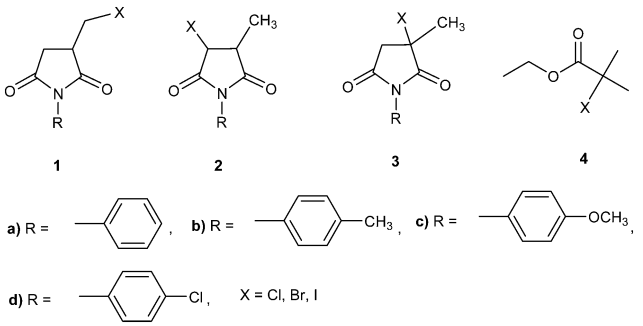

Fig. 2 The alkyl halides, **1** (**1a**-X to **1d**-X), **2** (**2a**-X to **2d**-X), **3** (**3a**-X to **3d**-X), and **4**-X (X = Cl, Br, I) investigated in this study.

and MMA (including the synthesized alkyl bromides **1a**-Br, **2a**-Br, and **3a**-Br), and (b) some common ATRP initiators (series **4**). The effect of the structure (*e.g.*, primary, secondary, and tertiary alkyl halides), substituent, and medium on the R–X bond dissociation of these alkyl halides was studied, and a comparison of their performance with known potential initiators was evaluated. All the gas phase-optimized geometries (Cartesian coordinates) of the studied compounds and radicals are given in ESI Tables S1 and S2,† respectively.

Structural features of alkyl halides and alkyl radicals

We used the B3LYP/6-31+G(d)/LanL2DZ method in our study. This level of theory has been used in the literature for studying similar processes.[20a–c] To check the accuracy of our computational results, we compared the selected IR frequencies and calculated ^{1}H NMR values with those obtained from experiments with the alkyl bromides **1a**-Br, **2a**-Br, and **3a**-Br. Correlation plots between experimentally determined and theoretically calculated values for selected IR frequencies and ^{1}H NMR of these alkyl bromides are displayed in Fig. 3 and 4, respectively. We found a good correlation between the experimentally determined and theoretically calculated IR frequency values (Fig. 3, $R^2 = 0.99$) and ^{1}H NMR δ values (Fig. 4, $R^2 = 0.99$). This indicates that the chosen method of calculation is quite appropriate for the studied compounds.

The R–X bond distances (r_{R-X}) for the studied compounds in gas phase as well as in two polar solvents are given in Table 2. They are between the ranges 1.809 Å to 2.202 Å for series **1**, 1.821 Å to 2.224 Å for series **2**, 1.844 Å to 2.261 Å for series **3**, and 1.855 Å to 2.278 Å for series **4** alkyl halides. The R–X bond distances follow the trends **1** < **2** < **3** < **4** for a given X and Cl < Br < I for a given series. The R–X bond lengths systematically increase for all the studied alkyl halides with increasing polarity of the medium and follow the trend gas phase < anisole < acetonitrile for a given R–X. The dihedral angles for the R–X bond with respect to the ring (or with respect to C(O)OC$_2$H$_5$ for **4**) are between 137°–177° for series **1** and **4**, and between 171°–172° for series **2** and **3**. The carbon atom bearing the unpaired electron for all the radicals was found to be planar in the sense that the sum of the three bond angles at this carbon was found to be 360° in all cases. The spin densities at this carbon varied from 0.87 to 1.17 in the order **1** > **2** > **3** ≈ **4**.

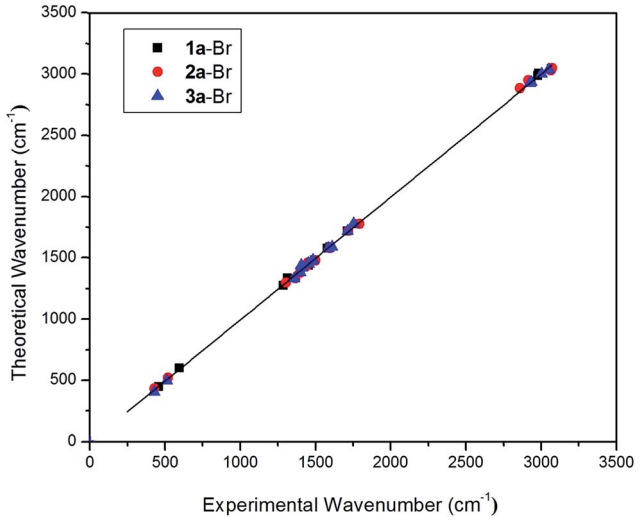

Fig. 3 Correlation plot of theoretical and experimental values of selected IR frequencies (in cm^{-1}) of the studied alkyl bromides. Frequencies corresponding to C–C (both aliphatic and aromatic), C=C (aromatic), C–H (both aliphatic and aromatic), C=O, C–N, and C–Br are considered.

Homolytic bond dissociation enthalpies and free energies

The bond dissociation enthalpy (BDE) data for the studied compounds is displayed in Table 3. They range from 304.25 kJ mol^{-1} to 170.64 kJ mol^{-1} for series **1**, 263.26 kJ mol^{-1} to 127.72 kJ mol^{-1} for series **2**, 250.70 kJ mol^{-1} to 108.96 kJ mol^{-1} for series **3**, and 257.07 kJ mol^{-1} to 115.16 kJ mol^{-1} for series **4** alkyl halides in gas phase. The R–X homolytic BDEs of alkyl chlorides were found to be higher than the corresponding alkyl bromides, which are in turn higher than their iodide counterparts. This variation is parallel to the decreasing ionic character of halides, Cl > Br > I. The decrease in BDEs was approximately 3–22 kJ mol^{-1} from Cl to Br, but approximately 110–140 kJ mol^{-1} from

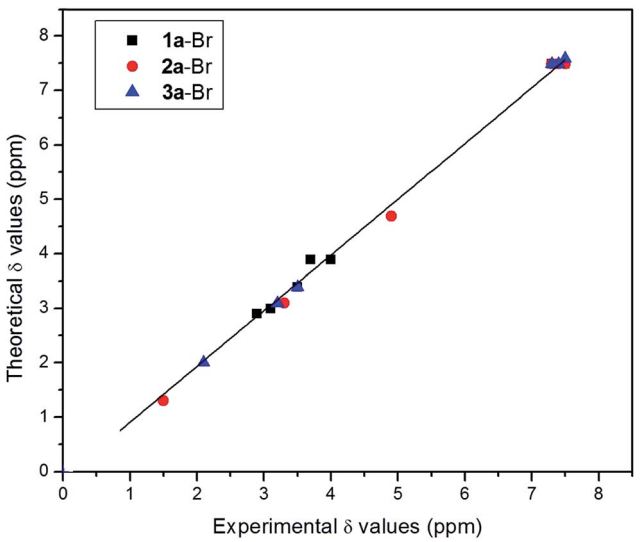

Fig. 4 Correlation plot of theoretical and experimental δ (in ppm) values of ^{1}H NMR of studied alkyl bromides.

Table 2 The R–X bond lengths of studied alkyl halides in gas phase and solution phase at 25 °C

	r_{R-X} (Å)		
R–X	Gas	Anisole	Acetonitrile
1a-Cl	1.809	1.817	1.822
1a-Br	1.966	1.973	1.977
1a-I	2.203	2.210	2.213
1b-Cl	1.810	1.818	1.822
1b-Br	1.966	1.973	1.977
1c-Cl	1.810	1.818	1.822
1c-Br	1.967	1.974	1.977
1c-I	2.203	2.267	2.270
1d-Cl	1.809	1.817	1.821
1d-Br	1.965	1.972	1.977
1d-I	2.202	2.202	2.213
2a-Cl	1.821	1.824	1.825
2a-Br	1.979	1.981	1.982
2a-I	2.225	2.227	2.228
2b-Cl	1.821	1.824	1.825
2b-Br	1.979	2.014	2.016
2c-Cl	1.822	1.825	1.826
2c-Br	1.979	1.982	1.982
2c-I	2.225	2.227	2.229
2d-Cl	1.821	1.824	1.825
2d-Br	1.978	1.980	1.981
2d-I	2.224	2.226	2.228
3a-Cl	1.844	1.848	1.850
3a-Br	2.008	2.014	2.016
3a-I	2.262	2.266	2.267
3b-Cl	1.844	1.848	1.849
3b-Br	2.009	2.014	2.016
3c-Cl	1.845	1.849	1.851
3c-Br	2.009	2.013	2.016
3c-I	2.263	2.267	2.270
3d-Cl	1.844	1.847	1.849
3d-Br	2.008	2.013	2.015
3d-I	2.261	2.266	2.269
4-Cl	1.855	1.865	1.869
4-Br	2.017	2.025	2.029
4-I	2.278	2.287	2.292

Br to I, for a given series. For a given halide, the trend in BDEs was **3** ≈ **4** < **2** < **1**, which is nearly according to the stability of the corresponding alkyl free radical generated. The BDE increases as we go from series **2** to series **1** as compared to going from series **3** to **2**. For a given series of alkyl halides, the BDEs decrease while the corresponding R–X bond distance increases (Table 2) as we go from X = Cl to X = I. The BDEs correlate well with the R–X bond lengths; as the R–X bond length increases, the BDEs decrease (Fig. 5). Solvent polarity has a different effect for 1° (series **1**) alkyl halides than 2° and 3° alkyl halides. The trends are gas phase > anisole > acetonitrile for **2**, **3** and **4** series alkyl halides, while the trend is gas phase < anisole < acetonitrile for series **1** alkyl halides. Thus, with increasing polarity of the medium, the relatively stable radicals (the **2**, **3** and **4** series) become more unstable, while the less stable radical **1** series becomes more stable.

The free energies for the studied alkyl halides (Table 3) exhibit nearly a constant difference with the enthalpy data (approximately 42 kJ mol^{-1} for series **1**, **2**, **3** and approximately 48 kJ mol^{-1} for series **4**). This indicates that the entropy factor contributing to the series **1**, **2**, and **3** alkyl halides (and similarly for the series **4**) is nearly the same. This is understandable from the structural similarities among alkyl halides of series **1**, **2**, and **3** (and similarly, series **4**). The free energies vary according to **4** ≈ **3** < **2** < **1** for a given X and follows the trends Cl > Br > I for a given series. The free energies, like BDEs, increase with decreasing R–X bond lengths. This is obvious from the correlation plot (Fig. 6) between the free energies and enthalpies. In the presence of polar solvents, the variation of free energies follows the trends gas phase > anisole > acetonitrile for the **2**, **3**, and **4** series alkyl halides, while it is gas phase < anisole < acetonitrile, for series **1** alkyl halides. This trend is similar to the trends found in BDEs.

Relative equilibrium constants (K_{ATRP})

As discussed in the introduction, the overall equilibrium constant (K_{ATRP}) can be given as the product of two equilibrium

Table 3 Enthalpy and free energy for R–X homolytic cleavage of studied alkyl halides in gas phase and solution phase at 25 °C

	ΔH (kJ mol^{-1})			ΔG (kJ mol^{-1})		
R–X	Gas	Anisole	Acetonitrile	Gas	Anisole	Acetonitrile
1a-Cl	304.25	309.03	312.42	262.30	267.55	270.73
1a-Br	282.14	285.92	289.09	240.78	243.14	247.92
1a-I	171.1	173.88	176.37	130.99	132.72	135.14
1b-Cl	304.29	306.67	312.67	262.92	273.03	271.26
1b-Br	282.54	284.00	289.42	244.74	254.1	248.66
1c-Cl	304.51	309.27	312.75	263.29	266.56	266.54
1c-Br	282.65	286.18	289.48	241.11	242.47	243.93
1c-I	171.31	174.16	176.77	131.45	133.45	133.62
1d-Cl	303.79	323.71	312.62	262.23	278.44	272.18
1d-Br	281.88	285.78	289.21	240.34	243.22	246.32
1d-I	170.64	173.72	176.46	130.64	134.26	135.03
2a-Cl	263.26	261.18	260.68	223.23	221.16	220.06
2a-Br	252.48	249.94	249.11	212.67	210.36	209.71
2a-I	128.76	126.04	125.23	89.49	87.24	86.62
2b-Cl	263.55	—	260.93	223.58	—	216.27
2b-Br	253.05	—	251.99	211.54	—	200.68
2c-Cl	263.56	261.67	261.14	223.80	222.49	219.97
2c-Br	252.86	250.51	249.56	213.15	212.15	209.36
2c-I	129.05	126.47	125.8	89.70	87.43	87.31
2d-Cl	262.22	260.06	259.76	222.29	220.69	223.86
2d-Br	251.6	248.79	248.34	211.83	208.9	208.93
2d-I	127.72	125.24	124.59	88.14	86.13	85.24
3a-Cl	250.7	247.39	245.92	208.66	204.27	202.69
3a-Br	247.88	243.71	242.06	205.12	199.94	198.21
3a-I	110.61	106.07	104.31	68.86	64.63	64.28
3b-Cl	251.07	247.62	246.46	208.01	204.38	203.1
3b-Br	248.42	244.18	242.59	206.26	199.3	197.32
3c-Cl	251.48	248.16	246.66	209.61	207.29	203.48
3c-Br	248.7	245.02	243.04	205.76	201.86	196.88
3c-I	110.83	106.47	104.8	69.54	64.95	63.82
3d-Cl	249.42	245.81	244.9	207.07	202.72	203.66
3d-Br	246.95	242.58	241.26	204.06	198.95	197.71
3d-I	108.96	104.45	102.84	67.58	62.81	62.26
4-Cl	257.07	255.98	255.53	209.9	208.81	205.31
4-Br	247.87	246.44	245.9	200.87	199.29	195.68
4-I	115.16	112.71	111.66	69.3	66.64	62.98

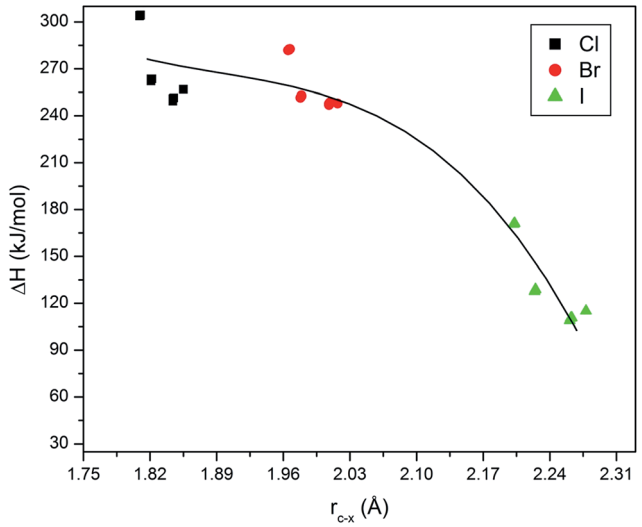

Fig. 5 Correlation plot of bond dissociation enthalpies with R–X bond distances of the studied alkyl halides.

constants, K_{RX} and K_X; the latter depends on a catalytic system and halogen radical. Thus, for a given catalytic system and a given X, K_X will be a constant, and the relative value of K_{ATRP} can be obtained from K_{RX}. We have calculated the K_{RX} of the alkyl halides from their free energy using a standard textbook formula.[43] We estimated the $K_X = (K_{ATRP}/K_{RX})$ values for the series **4** alkyl halides from their literature K_{ATRP} values (1.50×10^{-6} for **4**-Cl,[7] 3.93×10^{-9} for **4**-Br,[15b] and 2.2×10^{-8} for methyl-2-iodopropanoate[7]) and then used this K_X value for the rest of the compounds of a given X. We could have used the K_{ATRP} value of **4**-Br that was determined experimentally in this work for this purpose. However, for chlorides and iodides, only the literature values were used. Thus, we decided to use the literature values for all the studied alkyl halides. The values of K_{ATRP}, so obtained, are displayed in Table 4. A quick glance at Table 4 shows that the values of K_{ATRP} for the studied alkyl halides differ

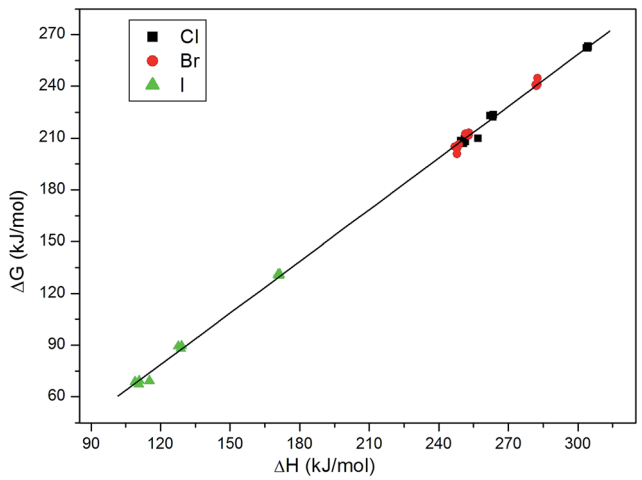

Fig. 6 Variation of enthalpies with the free energies for the R–X bond dissociation process for the studied alkyl halides.

in orders of magnitude of 10^{-4} to 10^{-16} for the gas phase at 25 °C. All of the alkyl halides of series **3** and many from series **2** (**2a**-Cl, **2b**-Cl, **2c**-Cl, **2d**-Cl, **2a**-I, **2b**-I, **2c**-I, and **2d**-I) have comparable K_{ATRP} values with those of corresponding commercial initiators (series **4**). However, the alkyl halides of series **1** have K_{ATRP} values much smaller than those of series **4** alkyl halides. The K_{ATRP} data follows trends **4** ≈ **3** > **2** >> **1** for a given X, and Cl < Br < I for a given series. With increasing temperature from 25 °C to 80 °C, the values of K_{ATRP} increase by an order of magnitude (10^3 to 10^9). A different substituent in the phenyl ring at the *para* position has no significant effect on bond lengths, bond dissociation enthalpy (BDEs), free energy, or the K_{ATRP} of the **1**, **2**, and **3** series of alkyl halides. If the medium of the system is changed, the trends of K_{ATRP} shift from gas phase > anisole > acetonitrile for series **1** alkyl halides, and gas phase < anisole < acetonitrile for the rest of the alkyl halides (series **2**, **3**, and **4**). We obtained good correlation in the variation of K_{ATRP} and R–X bond lengths as well as variation of K_{ATRP} with BDEs. These correlation plots are displayed in Fig. 7 and 8, respectively. Fig. 7 implies that as the R–X bond length increases, $-\log K_{ATRP}$ decreases, *i.e.*, $\log K_{ATRP}$ increases. This occurs because as the R–X bond length increases (bond weakens), homolysis is easier, and therefore, K_{ATRP} increases. Thus, iodides are better initiators than bromides, which in turn, are better initiators than chlorides. However, for a given X, there is little variation in the R–X bond length, yet there is an order of magnitude difference in K_{ATRP}. This is mainly due to the structural difference (primary, secondary, and tertiary) of alkyl halides. A similar explanation holds for the correlations between BDEs and K_{ATRP} as shown in Fig. 8.

The experimentally determined and theoretically calculated values of K_{ATRP} for the studied alkyl bromides were found to be comparable. The reported experimentally calculated K_{ATRP} value for **4**-Br is 3.93×10^{-09}, which is quite comparable with our experimentally calculated value of 1.29×10^{-09}. Similarly, the theoretically calculated K_{ATRP} values in acetonitrile at 25 °C for **1a**-Br, **2a**-Br, and **3a**-Br are 2.77×10^{-18}, 1.37×10^{-11}, and 1.42×10^{-09}, respectively, which are in good agreement with our experimentally determined K_{ATRP} values (1.14×10^{-18}, 1.18×10^{-11}, and 1.40×10^{-09}, respectively). The results are summarized in Table 1. All the observations of experimentally determined values of K_{ATRP} for the above mentioned alkyl bromides (using the Fischer–Fukuda equation for the persistent radical effect) are given in ESI Fig. S17 to S25.†

The K_{ATRP} values for **3a**-Br were found to be comparable with the commercially available initiator **4**-Br. Hence, ATRP was carried out using this initiator with the modified procedure (AGET-ATRP) to overcome the sensitivity of the catalyst (Cu^IBr) towards air and other oxidants.

AGET-ATRP of PI and MMA using 3a-Br as an initiator

The copolymerization of the monomers PI and MMA was carried out using the mole fraction ratio of 2 : 8 in the presence of $CuBr_2$/Bpy/$Sn(EH)_2$ in anisole at 80 °C using **3a**-Br as the initiator. The percent conversion of monomer was calculated gravimetrically by pouring the reaction mixture after 5 h, 10 h,

Table 4 Relative values of K_{ATRP} for R–X homolytic bond cleavage of studied alkyl halides in gas phase and in solution phase

	K_{ATRP}			
R–X	Gas, 25 °C	Gas, 80 °C	Anisole, 25 °C	Acetonitrile, 25 °C
1a-Cl	9.92×10^{-16}	2.03×10^{-07}	7.68×10^{-17}	5.19×10^{-18}
1a-Br	4.00×10^{-16}	1.86×10^{-08}	8.18×10^{-17}	2.77×10^{-18}
1a-I	1.18×10^{-15}	5.59×10^{-11}	5.30×10^{-11}	6.96×10^{-17}
1b-Cl	7.72×10^{-16}	1.58×10^{-07}	8.40×10^{-18}	4.18×10^{-18}
1b-Br	8.11×10^{-17}	4.32×10^{-09}	9.82×10^{-19}	2.06×10^{-18}
1c-Cl	6.65×10^{-16}	1.38×10^{-07}	1.14×10^{-16}	2.81×10^{-17}
1c-Br	3.50×10^{-16}	1.86×10^{-08}	1.07×10^{-16}	1.39×10^{-17}
1c-I	9.82×10^{-16}	4.71×10^{-11}	1.76×10^{-16}	1.28×10^{-16}
1d-Cl	1.02×10^{-15}	2.03×10^{-07}	9.50×10^{-19}	2.89×10^{-18}
1d-Br	4.78×10^{-16}	2.42×10^{-08}	7.92×10^{-17}	5.30×10^{-18}
1d-I	1.36×10^{-15}	6.25×10^{-11}	1.27×10^{-16}	7.26×10^{-17}
2a-Cl	6.94×10^{-09}	1.07×10^{-01}	1.03×10^{-08}	3.90×10^{-09}
2a-Br	3.36×10^{-11}	2.62×10^{-04}	4.53×10^{-11}	1.37×10^{-11}
2a-I	2.20×10^{-08}	7.21×10^{-05}	2.20×10^{-08}	2.20×10^{-08}
2b-Cl	6.02×10^{-09}	9.45×10^{-02}	—	1.80×10^{-08}
2b-Br	5.31×10^{-11}	2.01×10^{-04}	—	5.25×10^{-10}
2c-Cl	5.50×10^{-09}	8.65×10^{-02}	6.01×10^{-09}	4.04×10^{-09}
2c-Br	2.77×10^{-11}	2.22×10^{-04}	2.20×10^{-11}	1.58×10^{-11}
2c-I	2.02×10^{-08}	6.73×10^{-05}	2.04×10^{-08}	1.67×10^{-08}
2d-Cl	1.01×10^{-08}	1.46×10^{-01}	1.24×10^{-08}	8.42×10^{-10}
2d-Br	4.72×10^{-11}	3.49×10^{-04}	8.16×10^{-11}	1.88×10^{-11}
2d-I	3.79×10^{-08}	1.16×10^{-04}	3.44×10^{-08}	3.84×10^{-08}
3a-Cl	2.47×10^{-06}	$1.72 \times 10^{+01}$	9.36×10^{-06}	4.30×10^{-06}
3a-Br	7.06×10^{-10}	4.11×10^{-03}	3.03×10^{-09}	1.42×10^{-09}
3a-I	9.05×10^{-05}	9.46×10^{-02}	2.01×10^{-04}	2.00×10^{-04}
3b-Cl	3.22×10^{-06}	$2.30 \times 10^{+01}$	8.96×10^{-06}	3.65×10^{-06}
3b-Br	4.46×10^{-10}	2.64×10^{-02}	3.93×10^{-09}	2.03×10^{-09}
3c-Cl	1.68×10^{-06}	$1.23 \times 10^{+01}$	2.77×10^{-06}	3.13×10^{-06}
3c-Br	5.46×10^{-10}	3.35×10^{-03}	1.40×10^{-09}	2.42×10^{-09}
3c-I	6.89×10^{-05}	7.30×10^{-02}	1.76×10^{-04}	2.17×10^{-04}
3d-Cl	4.70×10^{-06}	$3.01 \times 10^{+01}$	1.75×10^{-05}	2.91×10^{-06}
3d-Br	1.08×10^{-09}	6.17×10^{-03}	4.52×10^{-09}	1.73×10^{-09}
3d-I	1.52×10^{-04}	1.43×10^{-01}	4.19×10^{-04}	4.07×10^{-04}
4-Cl	1.50×10^{-06}	$1.56 \times 10^{+01}$	1.50×10^{-06}	1.50×10^{-06}
4-Br	3.93×10^{-09}	2.29×10^{-02}	3.93×10^{-09}	3.93×10^{-09}
4-I	7.59×10^{-05}	1.05×10^{-01}	8.93×10^{-05}	3.05×10^{-04}

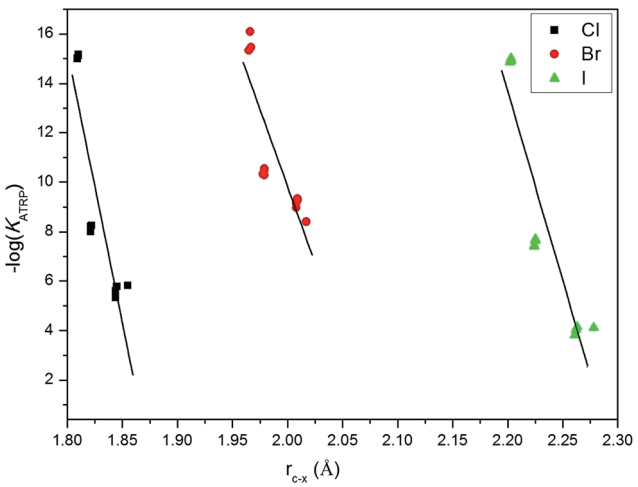

Fig. 7 Correlation plot of relative K_{ATRP} values with R–X bond lengths for the studied alkyl halides.

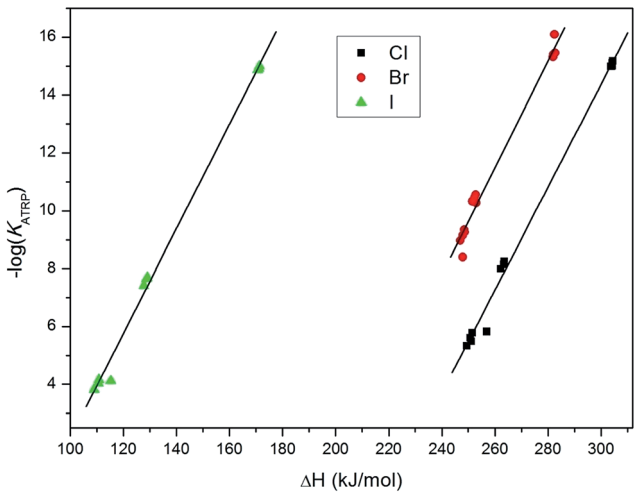

Fig. 8 Correlation plot of relative K_{ATRP} values with R–X bond enthalpies of studied alkyl halides.

15 h, 20 h, 25 h, 30 h, 35 h, 45 h, and 50 h in methanol. The copolymer that precipitated out was washed with hot methanol, dried, and weighed. The FTIR spectrum of the PI-MMA copolymer (ESI Fig. S26†) shows the >C═C< stretching of the phenyl ring at 1598, 1501, and 1456 cm^{-1}, pinpointing the incorporation of the phenylitaconimide in the copolymer. The absence of characteristic absorption bands at 1663–1665 cm^{-1} due to >C═C< bond stretching indicates the absence of monomers. The characteristic absorption bands at 1789 and 1714 cm^{-1} are due to carbonyl groups of imide (>C═O of imide), the absorption peak at 1229 cm^{-1} is due to C–O stretching of MMA, and the peak at 2850 cm^{-1} is due to the C–H stretch of $-CH_3$. In the ^1H NMR spectrum of the PI-MMA copolymer in $CDCl_3$ (ESI Fig. S27†), the peaks in the region $\delta = 7.6$–7.2 ppm are due to the phenyl ring of PI. The $-OCH_3$ of the side chain is observed at $\delta = 3.8$ ppm, whereas the signal at $\delta = 3.6$ ppm may be attributed to the methylene group adjacent to the carbonyl group of the side chain. Similarly, the $-CH_3$ of the side chain is observed at $\delta = 0.8$ ppm. The two methylene groups of the polymer

Table 5 The variation in molecular weight, PDI of copolymer, and % conversion of monomer with time for copolymerization of PI and MMA *via* AGET-ATRP. Experimental conditions: [PI]/[MMA]/[**3a**-Br]/[$CuBr_2$]/[Bpy]/[$Sn(EH)_2$] = 20/80/1/1/3/0.5, in anisole at 80 °C

S. no.	Time (h)	Yield (%)	% Conversion	Molecular weight (M_n) g mol^{-1}	PDI
1	5	17.89	17	3292	1.32
2	10	25.89	25	4316	1.56
3	15	34.75	35	4858	1.50
4	20	43.61	43	5086	1.37
5	25	55.03	54	6772	1.32
6	30	64.91	65	7167	1.34
7	35	73.25	73	8174	1.41
8	40	80.40	80	10 518	1.53
9	45	90.97	90	12 347	1.47
10	50	98.81	98	13 224	1.30

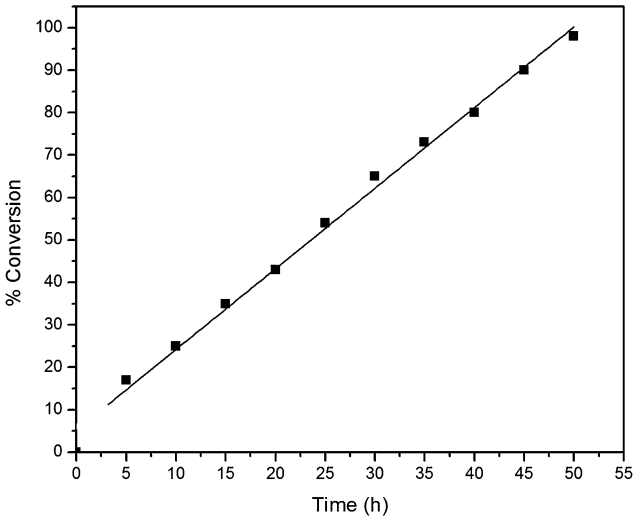

Fig. 9 Plot of % conversion of monomer with time for AGET-ATRP of PI and MMA. Experimental conditions: [PI]/[MMA]/[**3a**-Br]/[$CuBr_2$]/[Bpy]/[$Sn(EH)_2$] = 20/80/1/1/3/0.5, in anisole at 80 °C.

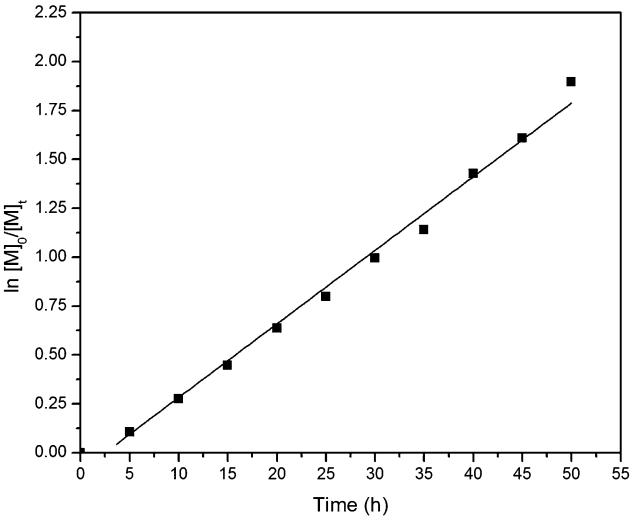

Fig. 11 Plot of ln{$[M]_0/[M]_t$} with time for AGET-ATRP of PI and MMA. Experimental conditions: [PI]/[MMA]/[**3a**-Br]/[$CuBr_2$]/[Bpy]/[$Sn(EH)_2$] = 20/80/1/1/3/0.5, in anisole at 80 °C.

backbone are observed in the region δ = 2.8–1.7 ppm and δ = 1.4–0.9 ppm, respectively.

The molecular weights of the copolymers were determined using GPC. The details of the percent conversion of monomers, polydispersity index (PDI), and molecular weights are given in Table 5. A typical linear variation in the plots of % conversion of monomers with time (Fig. 9) is observed, which is characteristic of controlled radical polymerization. The molecular weight of the copolymer also increases linearly with % conversion of monomers (Fig. 10). The concentration of the unreacted monomer (PI) in the reaction mixture was determined using ^{1}H NMR spectra of the reaction mixture recorded at various time intervals in the presence of a known amount of the standard, 1,1,2,2-tetrachloroethane. For the concentration determination of PI, the intensity of the peaks at δ = 6.5 was compared with the peaks for the standard at δ = 5.9 ppm. A linear plot (Fig. 11) is observed for ln{$[M]_0/[M]_t$} *vs.* time, further confirming that the polymerization is occurring under controlled radical polymerization conditions. The ^{1}H NMR spectra of the reaction mixture for the copolymerization of PI and MMA in $CDCl_3$ at various time intervals are given in ESI Fig. S28.† The PDI of the copolymer of PI and MMA was found to be 1.30 with 98% monomer conversion.

Recently, we reported the ATRP of PI and MMA using **4**-Br as the initiator, where we achieve only 50% conversion of monomer with 1.40 PDI for copolymers.[22b] Compared to this, the current study demonstrates that the molecular weight of copolymer, PDI ratio, and % conversion of monomer have been improved using **3a**-Br as the initiator. In addition, **3a**-Br has better control over the polymerization of PI and MMA as compared to **4**-Br.

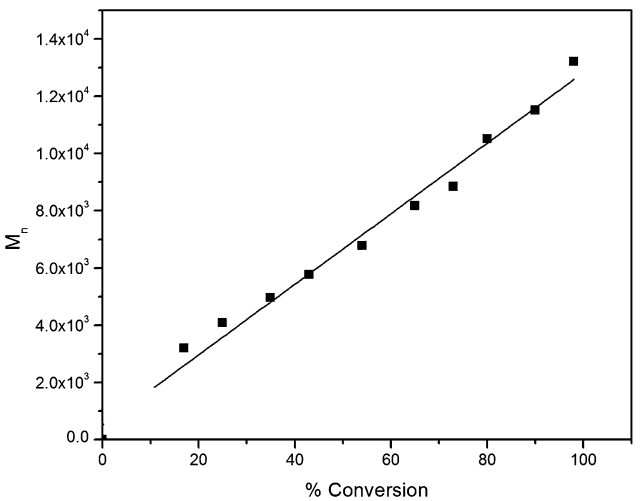

Fig. 10 Plot of molecular weight of copolymer with % conversion of monomer for AGET-ATRP of PI and MMA. Experimental conditions: [PI]/[MMA]/[**3a**-Br]/[$CuBr_2$]/[Bpy]/[$Sn(EH)_2$] = 20/80/1/1/3/0.5, in anisole at 80 °C.

Conclusions

We have reported the synthesis of three alkyl bromides (*N*-phenyl(3-bromo-3-methyl)succinimide, *N*-phenyl(3-bromo-4-methyl)succinimide, and *N*-phenyl(3-bromomethyl)succinimide) that are structurally similar to PI for possible chain initiation activity in the ATRP of PI and MMA. The K_{ATRP} of these alkyl bromides as well as a commercially available initiator (ethyl-2-bromoisobutyrate) was determined using UV-Vis-NIR spectroscopy, and k_t for radicals was determined using DOSY NMR spectroscopy.

We have also studied the structural and thermodynamic properties (bond dissociation enthalpies and free energies) of these alkyl bromides (along with some similar alkyl halides and some common ATRP initiators) using density functional theory. Variation of the substituent in the phenyl ring at the *para*

position of the studied alkyl halides has very little effect on bond length, bond dissociation enthalpy (BDEs), free energy, or K_{ATRP}. As expected, the R–X bond lengths increase in the order Cl < Br < I for a given R and **4** ≈ **3** < **2** < **1** for a given X, while the BDEs and free energies follow the opposite trends. With an increase in the polarity of the medium, the R–X bond distances increase (BDEs and free energies decrease) for series **2**, **3**, and **4**, while opposite trends are observed for series **1** (primary) alkyl halides. Relative values of K_{ATRP} were extracted from free energy values with respect to common ATRP initiators. It was found that values of K_{ATRP} slightly decrease with increasing solvent polarity and increase significantly with increasing temperature. The value of K_{ATRP} for series **3** and many of the alkyl halides of series **2** (**2a**-Cl, **2b**-Cl, **2c**-Cl, **2d**-Cl, **2a**-I, **2b**-I, **2c**-I, **2d**-I and two of the synthesized bromides **2a**-Br and **3a**-Br) are comparable to the commercially available initiator **4**-Br for the ATRP process.

We found good agreement between our experimentally determined and theoretically calculated K_{ATRP} values for **4**-Br, **1a**-Br, **2a**-Br, and **3a**-Br in acetonitrile at 25 °C. The copolymerization of PI and MMA was successfully carried out using one of our synthesized alkyl bromides, **3a**-Br, as the initiator in anisole at 80 °C *via* AGET-ATRP. Comparisons with our recent work on copolymerization of the same systems with the commercially available initiator **4**-Br demonstrates that our newly synthesized **3a**-Br performs more advantageously than **4**-Br in terms of controlling the rate of polymerization, % conversion of monomer, and PDI of obtained copolymers.

Acknowledgements

CD and RC are thankful to DST, New Delhi (Grant no. SR/FT/CS-053/2009) for funding. The support from BITS, Pilani – K. K. Birla Goa Campus is gratefully acknowledged. VSN wishes to thank the UGC, New Delhi for their support under XII Plan grants and Prof. S. G. Tilve, Department of Chemistry, Goa University for useful discussions.

References

1 (*a*) J.-S. Wang and K. Matyjaszewski, *J. Am. Chem. Soc.*, 1995, **117**, 5614; (*b*) M. Kato, M. Kamigaito, M. Sawamoto and T. Higashimura, *Macromolecules*, 1995, **28**, 1721; (*c*) M. Kamigaito, T. Ando and M. Sawamoto, *Chem. Rev.*, 2001, **101**, 3689.

2 K. Matyjaszewski and J. Xia, *Chem. Rev.*, 2001, **101**, 2921.

3 (*a*) *Controlled/Living Radical Polymerization, From Synthesis to Materials*, ed. K. Matyjaszewski, ACS Symposium Series 944, American Chemical Society, Washington, DC, 2006; (*b*) A. D. Jenkins, R. G. Jones and G. Moad, *Pure. Appl. Chem.*, 2010, **82**, 483.

4 (*a*) K. Matyjaszewski, *Macromolecules*, 2012, **45**, 4015; (*b*) D. J. Siegwart, J. K. Oh and K. Matyjaszewski, *Prog. Polym. Sci.*, 2012, **37**, 18.

5 (*a*) *Controlled/Living Radical Polymerization, Progress in ATRP, NMP, and RAFT*, ed. K. Matyjaszewski, ACS Symposium Series 768, American Chemical Society, Washington, DC, 2000; (*b*) C. J. Hawker, A. W. Bosman and E. Harth, *Chem. Rev.*, 2001, **101**, 3661; (*c*) C. Barner-Kowollik, T. P. Davis, J. P. Heuts, M. H. Stenzel, P. Vana and M. Whittaker, *J. Polym. Sci., Part A: Polym. Chem.*, 2003, **41**, 365.

6 N. V. Tsarevsky and K. Matyjaszewski, *Chem. Rev.*, 2007, **107**, 2270.

7 A. Mullar and K. Matyjaszewski, *Radical Polymerization, Controlled and Living Polymerization*, WILEY-VCH Verlag GmbH and Co. KGaA, Weinheim, 2009, pp. 103–166.

8 (*a*) T. Otsu, *J. Polym. Sci., Part A: Polym. Chem.*, 2000, **38**, 2121; (*b*) W. Zhang, C. Wang, D. Li, Q. Song, Z. Cheng and X. Zhu, *Macromol. Symp.*, 2008, **261**, 23; (*c*) R. Nicolay, Y. Kwak and K. Matyjaszewski, *Macromolecules*, 2008, **41**, 4585.

9 W. A. Braunecker and K. Matyjaszewski, *Prog. Polym. Sci.*, 2007, **32**, 93.

10 (*a*) M. E. Levere, N. H. Nguyen and V. Percec, *Macromolecules*, 2012, **45**, 8267; (*b*) N. H. Nguyen, M. E. Levere, J. Kulis, M. J. Monteiro and V. Percec, *Macromolecules*, 2012, **45**, 4606; (*c*) M. Zhong and K. Matyjaszewski, *Macromolecules*, 2011, **44**, 2668; (*d*) Y. Wang, M. Zhong, Y. Zhang and A. J. D. Magenau, *Macromolecules*, 2012, **45**, 8929; (*e*) Y. Wang, N. Soerensen, M. Zhong, H. Schroeder, M. Buback and K. Matyjaszewski, *Macromolecules*, 2013, **46**, 683.

11 (*a*) W. Tang and K. Matyjaszewski, *Macromolecules*, 2007, **40**, 1858; (*b*) B. M. Rosen and V. Percec, *J. Polym. Sci., Part A: Polym. Chem.*, 2008, **46**, 5663.

12 G. Odian, *Principles of Polymerization*, Wiley Interscience, Staten Island, 4th edn, 2004, pp.198–349.

13 G. Moineau, P. Dubois, R. Jerome, T. Senninger and P. Teyssie, *Macromolecules*, 1998, **31**, 545.

14 (*a*) W. Jakubowski and K. Matyjaszewski, *Macromolecules*, 2005, **38**, 4139; (*b*) K. Min, H. F. Gao and K. Matyjaszewski, *J. Am. Chem. Soc.*, 2005, **127**, 3825; (*c*) K. Min, H. F. Gao and K. Matyjaszewski, *J. Am. Chem. Soc.*, 2006, **128**, 10521.

15 (*a*) T. Pintauer, P. Zhou and K. Matyjaszewski, *J. Am. Chem. Soc.*, 2002, **124**, 8196; (*b*) W. Tang, N. V. Tsarevsky and K. Matyjaszewski, *J. Am. Chem. Soc.*, 2006, **128**, 1598; (*c*) W. Tang, Y. Kwak, W. Braunecker, N. V. Tsarevsky, M. L. Coote and K. Matyjaszewski, *J. Am. Chem. Soc.*, 2008, **130**, 10702; (*d*) D. A. Singleton, D. T. Nowlan, N. Jahed and K. Matyjaszewski, *Macromolecules*, 2003, **36**, 8609; (*e*) I. Degirmenci, S. Eren and V. Aviyente, *Macromolecules*, 2010, **43**, 5602; (*f*) A. P. Haehnel, M. Schneider-Baumann, K. U. Hiltebrandt, A. M. Misske and C. Barner-Kowollik, *Macromolecules*, 2013, **46**, 15.

16 (*a*) M. L. Coote, *Macromol. Theory. Simul.*, 2009, **18**, 388; (*b*) M. D. Miller and A. J. Holder, *J. Phys. Chem. A*, 2010, **114**, 10988.

17 K. Matyjaszewski, T. E. Patten and J. Xia, *J. Am. Chem. Soc.*, 1997, **119**, 674.

18 (*a*) H. Zang, B. Klumperman, W. Ming, H. Fischer and R. Linde, *Macromolecules*, 2001, **34**, 6169; (*b*) K. Ohno, Y. Tsujii, T. Miyamoto, T. Fukuda, M. Goto, K. Kobayashi and T. Akaike, *Macromolecules*, 1998, **31**, 1064; (*c*) H. Fischer, *Chem. Rev.*, 2001, **101**, 3581; (*d*) A. Goto and T. Fukuda, *Prog. Polym. Sci.*, 2004, **29**, 329; (*e*) H. Fischer, *J. Polym. Sci., Part A: Polym. Chem.*, 1999, **37**, 1885.

19 (*a*) W. A. Braunecker, N. V. Tsarevsky, A. Gennaro and K. Matyjaszewski, *Macromolecules*, 2009, **42**, 6348; (*b*) M. Horn and K. Matyjaszewski, *Macromolecules*, 2013, **46**, 3350–3357.

20 (*a*) M. B. Gillies, K. Matyjaszewski, P.-O. Norrby, T. Pintauer, R. Poli and P. Richard, *Macromolecules*, 2003, **36**, 8551; (*b*) C. Y. Lin, M. L. Coote, A. Gennaro and K. Matyjaszewski, *J. Am. Chem. Soc.*, 2008, **130**, 12762; (*c*) T. Guliashvili and V. Percec, *J. Polym. Sci., Part A: Polym. Chem.*, 2007, **45**, 1607; (*d*) C. Y. Lin, S. R. A. Marque, K. Matyjaszewski and M. L. Coote, *Macromolecules*, 2011, **44**, 7568.

21 (*a*) Z. Hu, X. Shen, H. Qiu, G. Lai, J. Wu and W. Li, *Eur. Polym. J.*, 2009, **45**, 2313; (*b*) H. Jiang, L. Zhang, J. Pan, X. Jiang, Z. Cheng and X. Zhu, *J. Polym. Sci., Part A: Polym. Chem.*, 2008, **50**, 2244; (*c*) H. Tang, M. Radosz and Y. Shen, *Macromol. Rapid Commun.*, 2006, **27**, 1127; (*d*) J. Mosnacek and M. Ilcikova, *Macromolecules*, 2012, **45**, 5859; (*e*) N. Chan, M. F. Cunningham and R. A. Hutchinson, *Macromol. Chem. Phys.*, 2008, **209**, 1797.

22 (*a*) C. Deoghare, R. N. Behera and R. Chauhan, "Controlled Radical Polymerization of *N*-phenylitaconimide with Methyl Methacrylate: Experimental and Theoretical Study" presented in 3rd FAPS Polymer Congress MACRO 2013, May 15–18, 2013, Bangalore, India; (*b*) C. Deoghare, P. C. Deb, C. Baby, R. N. Behera and R. Chauhan, "Controlled Radical Copolymerization of *N*-phenylitaconimide with Methyl Methacrylate *via* Atom Transfer Radical Polymerization" (Communicated to *J. Appl. Polym. Sci.*, manuscript reference number APP-2014-05-1917).

23 V. Anand and V. Choudhary, *J. Appl. Polym. Sci.*, 2003, **89**, 1195.

24 (*a*) V. Anand and V. Choudhary, *J. Appl. Polym. Sci.*, 2001, **82**, 2078; (*b*) R. Chauhan and V. Choudhary, *J. Appl. Polym. Sci.*, 2010, **115**, 491.

25 (*a*) P. Bonnarme, B. Gillet, A. M. Sepulchre, C. Role, J. C. Beloeil and C. Ducrocq, *J. Bacteriol.*, 1995, **177**, 3573; (*b*) K. Yahiro, S. Shibata, S.-r. Jia, Y. Park and M. Okabe, *J. Ferment. Bioeng.*, 1997, **84**, 375; (*c*) C. S. K. Reddy and R. P. Singh, *Bioresource Technol.*, 2002, **85**, 69.

26 (*a*) K. N. Ninan, R. George, K. Krishnan and K. V. C. Rao, *J. Appl. Polym. Sci.*, 1989, **37**, 127; (*b*) K. Y. Qiu and T. Zhao, *Polym. Inter.*, 1995, **38**, 71; (*c*) A. Solanki, V. Choudhary and I. K. Varma, *J. Appl. Polym. Sci.*, 2002, **84**, 2277.

27 (*a*) C. C. Price and E. C. Coyner, *J. Am. Chem. Soc.*, 1940, **62**, 1306; (*b*) O. Cakmak, I. Kahveci, I. Demirtas, T. Hökelek and K. Smith, *Collect. Czech. Chem. Commun.*, 2000, **65**, 1791.

28 E. O. Stejskal and J. E. Tanner, *J. Chem. Phys.*, 1965, **42**, 288.

29 D. Wu, A. Chen and C. S. Johnson Jr, *J. Magn. Reson. A*, 1995, **123**, 115.

30 C. S. Johnson Jr, *Prog. NMR Spectr.*, 1999, **34**, 203.

31 M. J. Frisch, G. W. Trucks, H. B. Schlegel, G. E. Scuseria, M. A. Robb, J. R. Cheeseman, G. Scalmani, V. Barone, B. Mennucci, G. A. Petersson, H. Nakatsuji, M. Caricato, X. Li, H. P. Hratchian, A. F. Izmaylov, J. Bloino, G. Zheng, J. L. Sonnenberg, M. Hada, M. Ehara, K. Toyota, R. Fukuda, J. Hasegawa, M. Ishida, T. Nakajima, Y. Honda, O. Kitao, H. Nakai, T. Vreven, J. A. Montgomery, Jr, J. E. Peralta, F. Ogliaro, M. Bearpark, J. J. Heyd, E. Brothers, K. N. Kudin, V. N. Staroverov, T. Keith, R. Kobayashi, J. Normand, K. Raghavachari, A. Rendell, J. C. Burant, S. S. Iyengar, J. Tomasi, M. Cossi, N. Rega, J. M. Millam, M. Klene, J. E. Knox, J. B. Cross, V. Bakken, C. Adamo, J. Jaramillo, R. Gomperts, R. E. Stratmann, O. Yazyev, A. J. Austin, R. Cammi, C. Pomelli, J. W. Ochterski, R. L. Martin, K. Morokuma, V. G. Zakrzewski, G. A. Voth, P. Salvador, J. J. Dannenberg, S. Dapprich, A. D. Daniels, O. Farkas, J. B. Foresman, J. V. Ortiz, J. Cioslowski and D. J. Fox, *Gaussian 09, Revision B.01*, Gaussian, Inc., Wallingford CT, 2010.

32 C. Lee, W. Yang and R. G. Parr, *Phys. Rev. B: Condens. Matter Mater. Phys.*, 1988, **37**, 785; A. D. Becke, *Phys. Rev. A: At., Mol., Opt. Phys.*, 1988, **38**, 3098; A. D. Becke, *J. Chem. Phys.*, 1993, **98**, 5648.

33 J. B. Foresman and A. Frisch, *Exploring chemistry with electronics structure methods*, Gaussian, Inc., Pittsburgh, 2nd edn, 1996, p. 64.

34 C. E. Moore, *Atomic Energy Levels*, US Government Printing Office, Washington, DC, 1952, vol. I–III.

35 S. Miertus, E. Scrocco and J. Tomasi, *Chem. Phys.*, 1981, **55**, 117.

36 V. Anand, S. Agarwal, A. Greiner and V. Choudhary, *Polym. Int.*, 2005, **54**, 823.

37 (*a*) H. Fischer and P. Henning, *Acc. Chem. Res.*, 1987, **20**, 200; (*b*) H. Fischer and L. Radom, *Angew. Chem., Int. Ed.*, 2001, **40**, 1340.

38 H. H. Schuh and H. Fischer, *Helv. Chim. Acta*, 1978, **61**, 2130.

39 J. H. Gorrell and J. T. Dubois, *Trans. Faraday Soc.*, 1967, **63**, 347.

40 (*a*) H. A. Kooijman, *Ind. Eng. Chem. Res.*, 2002, **41**, 3326; (*b*) In-C. Yeh and G. Hummer, *J. Phys. Chem. B*, 2004, **108**, 15873.

41 (*a*) T. Brand, E. J. Cabrita and S. Berger, *Prog. NMR Spectr.*, 2005, **46**, 159; (*b*) Y. Cohen, L. Avram and L. Frish, *Angew. Chem., Int. Ed.*, 2005, **44**, 520; (*c*) P. S. Pregosin, P. G. Anil Kumar and I. Fernandez, *Chem. Rev.*, 2005, **105**, 2977.

42 (*a*) M. S. Kharasch and W. M. M. Potts, *J. Org. Chem.*, 1937, **02**, 195; (*b*) M. S. Kharasch, H. Engelmann and F. R. Mayo, *J. Org. Chem.*, 1937, **02**, 288; (*c*) M. S. Kharasch and M. C. McNab, *J. Am. Chem. Soc.*, 1934, **56**, 1425; (*d*) M. S. Kharasch and J. A. Hinckley Jr, *J. Am. Chem. Soc.*, 1934, **56**, 1243.

43 P. Atkins and J. de Paula, *Physical Chemistry*, W. H. Freeman and Company, United States, 9th edn, 2010, p. 217.

